Research Papers

J. Synchrotron Rad. (2000). **7**, 361–367

Visualization, quantification and therapeutic evaluation of angiogenic vessels in cancer by synchrotron microangiography

Takafumi Sekka,[a] Svetlana A. Volchikhina,[a] Akira Tanaka,[a] Makoto Hasegawa,[a] Yutaka Tanaka,[a] Yasuo Ohtani,[a] Tomoo Tajima,[a] Hiroyasu Makuuchi,[a] Etsuro Tanaka,[a] Yoshiro Iwata,[a] Shinkichi Sato,[a] Kazuyuki Hyodo,[b] Masami Ando,[b] Keiji Umetani,[c] Misao Kubota,[d] Kenkichi Tanioka[d] and Hidezo Mori[a]*

[a]Departments of Surgery, Physiology, Radiology and Pathology, Tokai University School of Medicine, Isehara, Kanagawa, Japan, [b]National Laboratory for High Energy Physics, Tsukuba, Japan, [c]Synchrotron Radiation Research Institute, Mikazuki, Japan, and [d]Nippon Hoso Kyokai Science and Technical Research Laboratories, Tokyo, Japan. E-mail: coronary@keyaki.cc.u-tokai.ac.jp

(*Received 24 April 2000; accepted 7 August 2000*)

The usefulness of a synchrotron microangiography system for depicting, quantitating and therapeutically evaluating angiogenic vessels in cancer is illustrated. In 20 mice transplanted with murine colon cancer, sequential changes in the angiogenic vessels were determined by using synchrotron microangiography, using changes in tumor volume for reference. This system allowed the depiction and quantification of angiogenic vessels in the period from one to four weeks after transplantation. The effects of antiangiogenic therapy were evaluated by using a neutralizing antibody against vascular endothelial growth factor. The neutralizing antibody partially suppressed angiogenesis and tumor growth. Synchrotron microangiography is shown to be useful for the depiction, quantification and evaluation of angiogenic vessels in cancer.

Keywords: microangiography; cancer; antiangiogenic drugs; blood vessels.

1. Introduction

It is well known that angiographic visualization of the immature vascular network produced by angiogenesis is a crucial diagnostic procedure for distinguishing malignant tumors from benign tumors. Recently, antiangiogenic drugs have become expected to provide a novel form of cancer therapy, but being able to depict, quantitate and evaluate angiogenic vessels in cancer is essential for evaluating the effects of such drugs (Folkman, 1995). Conventional angiography, however, cannot demonstrate the characteristic angiographic features of small cancers well, and therefore does not allow evaluation of sequential changes in angiogenic vessels (Janet & Julie, 1995). A pancreatic cancer having a diameter of 2 cm or less is defined as an early stage of such cancers (Hermanek & Sobin, 1987). The immature vascular networks usually consist of vessels having a diameter of less than 200 μm (Warren, 1979; Ekelund, 1979). As current angiography systems are not suitable for demonstrating vessels with a diameter of less than 200 μm, angiographic demonstration of such an immature vascular network is difficult in tumors with a diameter of 2 cm or less. The purpose of the present study was to elucidate the usefulness of the microangiography system that we have developed, which uses monochromatic synchrotron radiation and a high-definition television (HDTV) camera system equipped with a high-sensitivity image pick-up tube (Mori *et al.*, 1994, 1996) for depicting small angiogenic vessels, quantitating the sequential changes in vessels for one to four weeks after transplantation, and evaluating the effects of antiangiogenic therapy by using a neutralizing antibody against vascular endothelial growth factor (VEGF) on the sequential changes in angiogenic vessels, as well as tumor size.

2. Materials and methods

2.1. *Synchrotron microangiographic system*

The synchrotron radiation angiographic system has already been described in previous reports (Mori *et al.*, 1994, 1996). Briefly, monochromatic synchrotron radiation having an energy level of 33.3 keV was obtained from beamlines NE-5 and BL-14 in the National Laboratory for High Energy Physics, Tsukuba, Japan (Hyodo *et al.*, 1991).

Applying a monochromatic 33.3 keV X-ray beam maximizes the difference in X-ray absorption between iodine contrast and body tissue. The monochromatic X-ray beam formed a contrast image of the object on a fluorescent screen (HR-mammo, Fuji Film, Tokyo, or FOS J6144, Hamamatsu Photonics, Shizuoka) (Fig. 1*a*). A 20.0–30.0 mm × 20.0 mm area was scanned at 15 or 30 frames s^{-1} for 6 s using an HD-TV camera equipped with an avalanche-type pick-up tube with 1125 TV lines (Tanioka *et al.*, 1988), and each frame consisted of a single field. The image was digitized to a resolution of 1024 × 1024 pixels and 10 or 12 bits $pixel^{-1}$, and stored on a digital video tape (HDD1000, SONY, Tokyo) and/or in a frame memory (DFM-P, Keisoku-Giken, Tokyo, or custom-made 192 mega-words of 12 bits, Zenisu Keisoku, Tokyo). A modulation-transfer-function chart study revealed that the system enables the identification of adjacent 20 line-pair mm^{-1} leadlines [Kyokko X-ray test chart type-14 (2–20 line-pair mm^{-1}), Kasei Optonix Ltd, Tokyo] (Umetani *et al.*, 1996). Assessment of contrast resolution using a vascular phantom (type 76–700, Nuclear Associates, New York) showed that the minimum vascular phantom (0.5 mm diameter) was visualized with a minimum concentration (2.5 mg ml^{-1} of iodine) through a 75 mm-thick acrylic block. Temporal subtraction could be performed between two still-frames just before and during injection of the contrast material to visualize small arteries feeding a cancer as clearly as possible. Linear interpolation between adjacent pixels was applied to perform quantitative analysis at a more effective pixel side length of 9.75 ± 0.05 μm (*i.e.* side length of the visual field: 2048 pixels) (Fig. 1*a*).

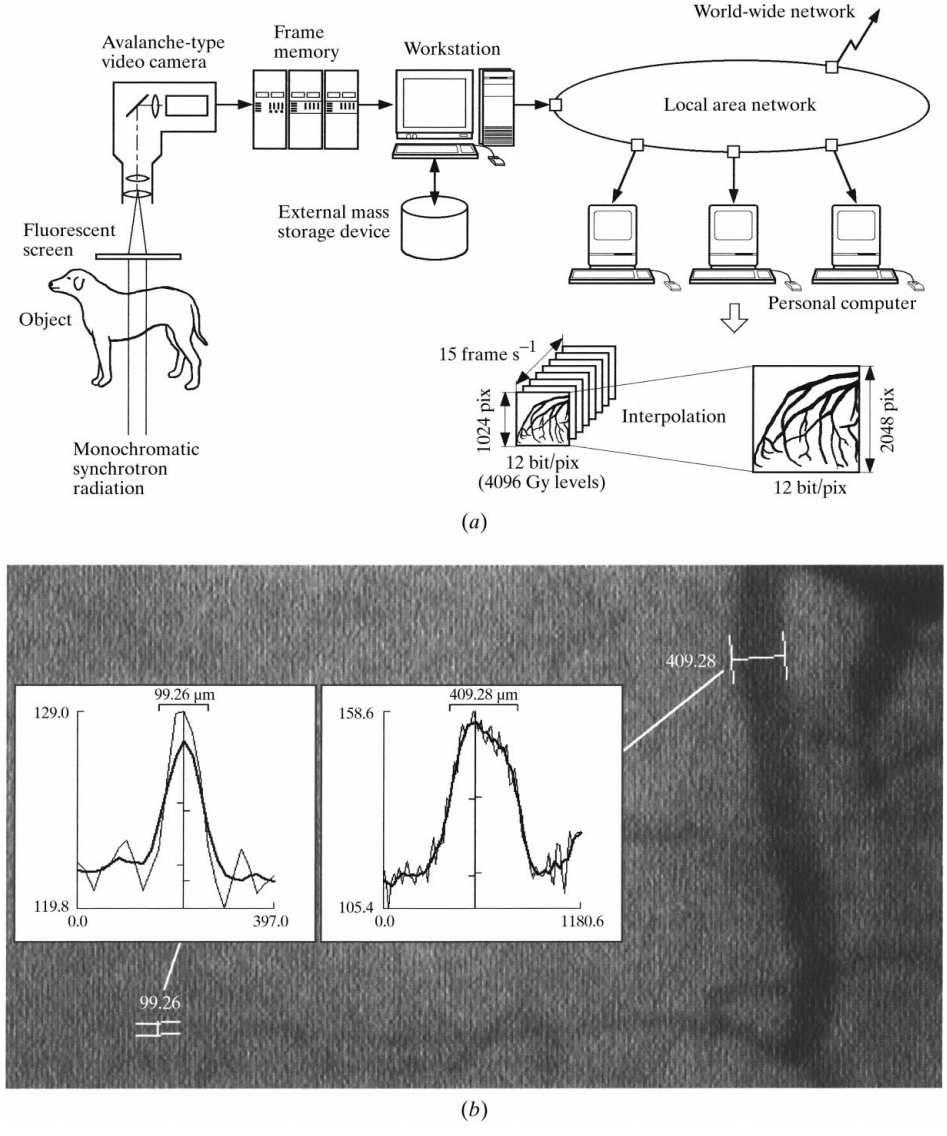

Figure 1
(*a*) Schematic representation of the synchrotron radiation microangiography system. (*b*) Schematic representation of the quantitative analytic methodology for vessel diameters.

2.2. *Quantitative analytic methodology for vessel diameters*

In spite of the improvements in digital images, conventional software packages for automated quantitative coronary angiography cannot accurately detect the contours of small vessels of less than 500 μm in diameter because of the poor contrast of small vessels (Tanaka *et al.*, 1997). We therefore quantified the vessel diameter using a public domain program (*NIH Image*, version 1.61, National Institutes of Health) by using a PASCAL-like built-in-macro programming language on a personal computer. The vessel diameter was calculated as follows. The operator initially clicked the button to enter the position and direction of a particular vessel segment. The personal computer calculated a density profile plot vertical (perpendicular) to the vessel segment (the thin profile plot in the inlets of Fig. 1*b*), and then smoothed it by averaging over three to seven adjacent points of the profile (the thick profile plot). Subsequently, the operator determined the left- and right-side background density levels of the smoothed profile plot, and entered them by clicking. The background levels on the left and right side were not usually identical. In the smoothed profile plot, the left-side contour was computed as a horizontal point corresponding to a mean level between the left background level and the apex. The right contour was computed in the same manner. Finally, the contours were drawn on the angiogram to confirm the computation (Fig. 1*b*). Owing to the almost parallel nature of the monochromatic synchrotron radiation beam, the geometric relationships among the light source, the object and the fluorescent screen did not affect the size of the vessel image on the fluorescent screen, and thus the diameter could be directly calibrated with the pixel size (9.75 ± 0.05 μm pixel^{-1}). Using this method, the mean diameter (± standard deviation) of a reference copper wire was measured as 131 ± 13 μm ($n = 31$), demonstrating a very small difference from its known diameter of 130 μm. Moreover, dual measurements of small vessels (37 vessels, 52–667 μm in diameter) by two independent observers were highly correlated ($r = 0.999$), as described in our previous paper (Tanaka *et al.*, 1999).

2.3. *Experimental protocol*

Sequential changes in tumor size and in the angiographic features of angiogenic vessels of the cancer were evaluated in 20 female BALB/c mice (Charles River Japan Inc., Yokohama, Japan), aged five to six weeks, into which colon cancer (Colon 26) had been transplanted. The mice were anesthetized with pentobarbital sodium (40 mg kg^{-1}) administered intraperitoneally (Nembutal, Abbott Laboratories, North Chicago, IL, USA), and the cancer cells

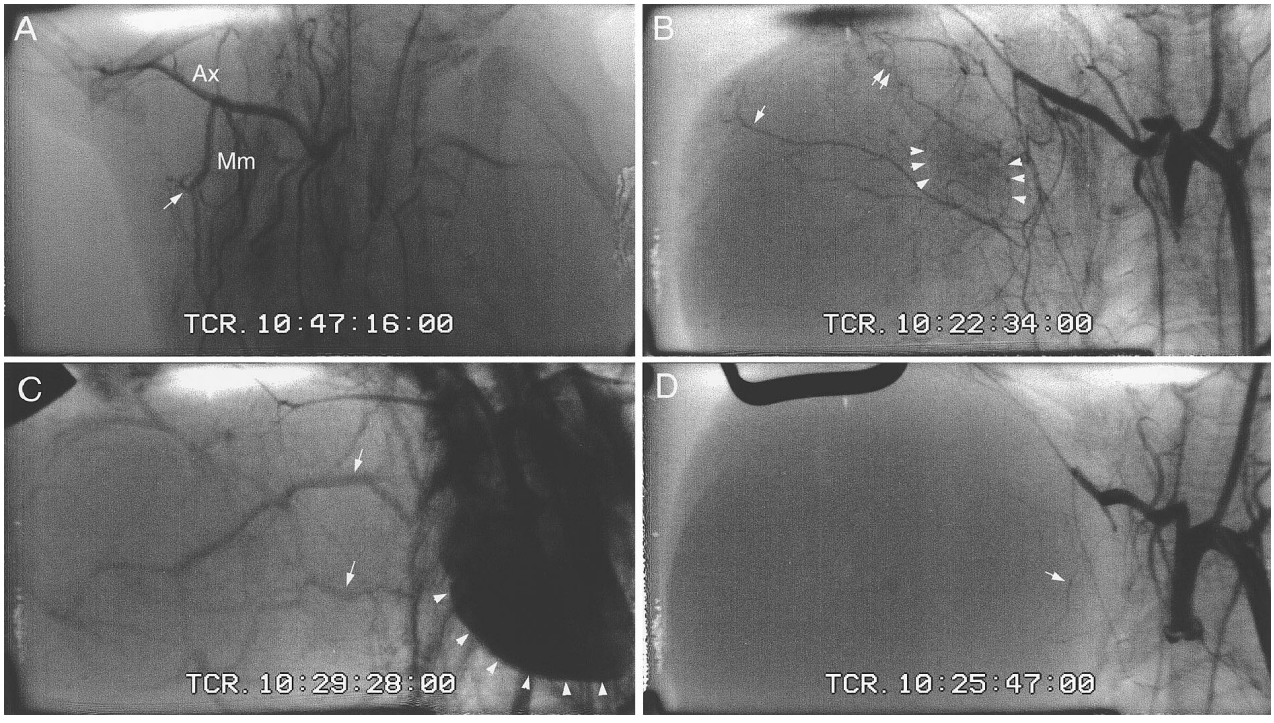

Figure 2
(*A*) Representative microangiogram from the control mice taken one week after transplantation. Growth of the tumor was not prominent. However, a small feeding artery from the mammary artery could be identified (white arrow). (*B*) Representative microangiogram from the control mice taken four weeks after transplantation. Tumor growth was marked, with a horizontal tumor diameter of approximately 15 mm (visual field: 20 × 30 mm). (*C*) Representative microangiogram from the control mice taken four weeks after transplantation. The tumor was fed not only by the mammary and axillary arteries but also by the pulmonary artery, which contains low-oxygen blood. (*D*) Representative microangiogram at four weeks after transplantation from the group treated with VEGF antibody. Growth of the networks of tumor feeding arteries is obviously suppressed compared with (*B*) from a control mouse.

Table 1
Angiographic findings of the feeding vessels of the tumor.

The table summarizes the number of proximal segments of the tumor arteries originating from the axillary or mammalian artery, their diameter and maximum order of branching, and the angiographic scores. Angiographic scores are not suitable for assessment of feeders from the pulmonary artery, because only a small number of vessels having a much wider diameter filled with low concentrations of contrast material could be identified. The tumors were arbitrarily divided into six regions: proximal, mid- and distal regions in the upper and lower half of the tumor. The pulmonary artery could be identified in an average of 4.6 of the six regions in the control mice at three to four weeks. The vascular score is defined using the vascular density score as: vascular score = $\sum_{i\ (\text{whole tumor})}(\text{vascular density score})_i\, ds_i$.

	Week	Number of mice	Number of primary branches	Diameter of primary branches (μm)	Maximum ordering of branching	Vascular score	Vascular density score (mm^{-2})	Feeding area
Axillary and mammary arteries								
Control	1–2	7	2.57 ± 1.21	168 ± 27	1.70 ± 0.65	8.5 ± 7.8	0.080 ± 0.063	Not analyzed
	3–4	7	5.86 ± 2.27†	175 ± 29	2.80 ± 0.75†	41.1 ± 21.3†	0.103 ± 0.046	Not analyzed
Anti-VEGF antibody	4	4	2.50 ± 0.58‡	197 ± 40	2.30 ± 0.96‡	16.5 ± 3.4‡	0.052 ± 0.043	Not analyzed
Pulmonary artery								
Control	1–2	11	0.00 ± 0.00	–	–	–	–	–
	3–4	4	1.50 ± 0.58	–	–	–	–	–
Anti-VEGF antibody	4	4	0.00 ± 0.00	–	–	–	–	–

† $P < 0.05$ *versus* control value at weeks 1–2. ‡ $P < 0.05$ *versus* control value at weeks 3–4 (by analysis of variance).

(Colon 26, 1×10^6 per 0.1 ml saline) were subcutaneously injected in the axillary region. The horizontal and vertical diameters of the tumor were measured every three days, and the volume was calculated by applying an ellipsoidal model. To investigate the preventive effect of VEGF neutralizing antibody on the growth of the transplanted colon cancer, 20 mice were divided into two groups: a group treated with VEGF antibody ($n = 5$) and a control group ($n = 15$). The experimental group received 0.2 ml of VEGF antibody (antimouse VEGF neutralizing antibody, R&D System Inc., USA) at a dose of 100 μg per mouse intraperitoneally on the seventh day after transplantation, and 0.1 ml of VEGF antibody at a dose of 10 μg per mouse twice a week by subcutaneous injection in the axillary region, while the control group received the same dose of Gout immunoglobulin (Gout IgG, Sigma BioScience, USA). Microangiography was performed once or twice at one, two, three or four weeks after transplantation. To perform microangiography the first time, the animals were anesthetized with sodium pentobarbital, an incision was made in the right cervical region, and a 24 gauge catheter was advanced into the innominate artery *via* the right common carotid artery. In 10 of the 20 mice, microangiography was performed a second time two weeks after the first angiography. To perform angiography the second time, the animals were similarly anesthetized, an incision was made in the right inguinal region to expose the right femoral artery, and the same catheter was advanced into the ascending aorta *via* the right femoral artery. The contrast material used for microangiography was 0.3 ml (0.1 ml s^{-1}) of a non-ionic contrast medium (Iopamidol 360, Nippon Schering, Osaka, Japan). After completion of the first or second microangiography, the animal was killed with an overdose of pentobarbital, and histological studies (Victoria blue-hematoxylin and eosin stain) were performed. All of the data are shown as means and standard deviation. Sequential changes in tumor volume were analyzed by two-way ANOVA (analysis of variance). Angiographic indices were compared between the groups by using the unpaired t-test. All of our experiments on animals conformed to the Tokai University School of Medicine Guide for the Care and Use of Laboratory Animals, which is based on the NIH guidelines.

3. Results

3.1. *Sequential angiographic changes in the arteries feeding the cancer*

Representative angiographic images of the transplanted tumors obtained by synchrotron radiation microangiography are shown in the four panels in Fig. 2. Panels *A*, *B* and *C* show differences in the microangiographic findings between one and four weeks after transplantation in the control mice. The contrast material injected into the ascending aorta visualized the networks of tumor-feeding arteries originating from the mammary artery even at one week after transplantation (panel *A*). In the angiogram taken after four weeks (panel *B*), tumor growth was marked, with a horizontal diameter of approximately 15 mm (visual field: 20 × 30 mm). The network of tumor-feeding arteries from both the mammary and axillary arteries has become more substantial than in panel *A*. In the vessel indicated by the arrow (panel *B*), fourth-order branches could be identified. The tumor-feeding vessel indicated by the double arrow exhibits the characteristic appearance of the vessels supplying malignant tumors, *i.e.* an undulating shape lacking side branches. The site indicated by the arrowheads shows abnormal staining. In another example at four weeks (panel *C*), the tumor was fed not only by these arteries but by the pulmonary artery, whose blood contains low oxygen levels. The vessels indi-

cated by the white arrow penetrate throughout the tumor. These vessels were not visualized immediately after the intra-aortic injection of the contrast material and only became visible after the right ventricle and main pulmonary arteries were opacified with contrast material. Table 1 summarizes the number of proximal segments of the arteries to the tumor originating directly from the axillary or mammary artery, their diameter and maximum order of branching, and the angiographic scores (vascular score and vascular density score), in addition to the pulmonary artery findings. The quantitative angiographic cancer vessel scores were calculated as follows. A composite of 3 mm × 3 mm grids was placed over the angiograms. The total number of grid intersections in the cancer and the total number of intersections crossed by a contrast-opacified artery were counted individually. The vascular density score for each film was calculated as the ratio of grid intersections crossed by opacified arteries to the total number of grid intersections in the cancer (number of vessels mm^{-2}). The vascular score is defined as the vascular density score times the number of grids in the tumor. Comparison of these indices between three to four weeks and one to two weeks in the control mice revealed a sequential increase in the number of primary branches of the vessels, the maximum order of their branchings and in the angiographic scores, but the diameter of the proximal site of the tumor-feeding artery was no different. At three to four weeks, the tumor was fed not only by the mammary and/or axillary arteries but also by the pulmonary artery, which contains low-oxygen blood. By contrast, at one to two weeks the networks of tumor-feeding arteries originated only from the mammary artery and/or axillary artery. Conventional angiography by X-ray tube (DH-1513TM, Hitachi, Tokyo, Japan) with a tube voltage of 65 keV and Image Intensifier-TV system failed to show any proximal arteries or their branches (data not shown). Fig. 3 shows the sequential changes in tumor volume. In the control mice (open squares), tumor volume increased sequentially ($P < 0.05$, two-way ANOVA, where P is the probability in statistical analysis).

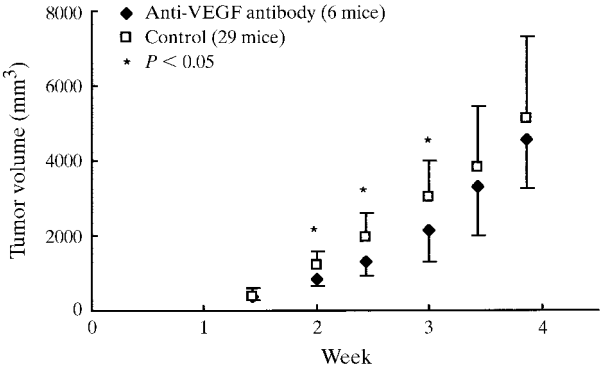

Figure 3
Sequential changes in tumor volume of Colon 26 mice colon cancer implanted in the right axillary region. The star symbol indicates a significant difference between the antibody-treated group and control group at 14, 17 and 21 days after transplantation (unpaired t-test). Value = mean ± standard deviation.

3.2. *Therapeutic effects of VEGF neutralizing antibody*

Panel *D* in Fig. 2 shows a representative microangiogram at four weeks after transplantation in the group treated with VEGF antibody. Compared with the image in panel *B* from the control mouse, growth of the networks of tumor-feeding arteries has obviously been suppressed. As summarized in Table 1, the number of feeding arteries, the maximum order of branching and the angiographic scores in the VEGF-antibody-treated mice at four weeks after transplantation (Ab4w) were significantly smaller than in the control group (Cntl3–4w). The diameter of the proximal segment, however, was not significantly different from the control mice at three to four weeks. No feeding originating in the pulmonary artery was noted in the VEGF group. As shown in Fig. 3, the tumor volume in the mice treated with VEGF antibody was significantly smaller than in the control group on days 14, 17 and 21 after transplantation ($P < 0.05$, two-way ANOVA). On days 9 and 26, however, the difference was not significant.

4. Discussion

4.1. *New observations*

Synchrotron microangiography was useful for the depiction, quantification and therapeutic evaluation of angiogenic vessels in a murine model of cancer. The system (Fig. 1) allowed depiction and quantification of angiogenic vessels in the period from one to four weeks after transplantation (panels *A–C* in Fig. 2 and Table 1). Anti-angiogenic therapy with neutralizing antibody against vascular endothelial growth factor revealed angiographic evidence for partial suppression of angiogenesis (panel *D* in Fig. 2 and Table 1), in addition to suppression of tumor growth (Fig. 3).

4.2. *Advantage of SRA and HD-TV*

The microangiographic system, using monochromatic synchrotron radiation and an HD-TV camera system with a high-sensitivity image pick-up tube, that was assessed in this study visualized immature vascular networks in transplanted malignant tumors (Colon 26), having diameters ranging from 6 mm × 6 mm to 23 mm × 21 mm and volumes ranging from 113 mm^3 to 5308 mm^3, in mice (Figs. 1 and 2). The immature vascular networks could not be demonstrated by conventional angiography (data not shown). Our angiographic system has two advantages over conventional angiography. The monochromatic synchrotron radiation having an energy of 33.3 keV allows detection of small amounts of iodine contrast in small vessels by maximizing the difference between the mass absorption coefficients of iodine and tissue. The detection system of conventional angiography is not oriented to the detection of small vessels having diameters of 200 μm or less, and

small-vessel radiography requires the use of a high-definition detector. However, setting small pixels in a high-definition detector is generally associated with a decrease in sensitivity, because the number of photons per pixel decreases. The present HD-TV camera system has a photoconductive layer containing amorphous selenium in the image pick-up tube, and at high voltages (1×10^6 V or more) an electron–hole pair produced by an incident photon is accelerated (avalanche phenomenon) (Tanioka *et al.*, 1988; Umetani *et al.*, 1996; Kubota *et al.*, 1996). This allows internal low-noise amplification with an effective quantum ratio of >600 (conversion ratio of photons to electrons). This allows the high-definition video camera to detect high-definition images without loss of sensitivity. This system can visualize small vessels of the heart, brain and digestive organs (Mori *et al.*, 1994, 1996), as well as small collateral arteries in ischemic limbs (Takeshita *et al.*, 1997). The digital processing described in the present paper improved the reproducibility of the measurements.

4.3. *Antiangiogenic cancer therapy and synchrotron radiation microangiography*

The growth of solid tumors is essentially dependent on angiogenesis (Folkman, 1972, 1990), and for this reason neovascularization mediated by growth factors produced by tumors is critical for their growth. VEGF is an endothelial-cell-specific mitogen and angiogenesis inducer released by a variety of tumor cells and expressed in human tumors *in situ.* Neutralizing anti-VEGF antibody has been reported to suppress the growth of many different kinds of tumors (Kim *et al.*, 1993). In this study the microangiograms taken three to four weeks after tumor transplantation in mice treated with neutralizing anti-VEGF antibody showed evidence of partial suppression of newly developed vessels and of tumor growth. On days 14, 17 and 21 after transplantation the tumor volume in the mice treated with VEGF antibody was significantly smaller than in the control group. On days 23 and 27 after transplantation, however, the significance of the difference between the VEGF antibody group and the control group disappeared. This appears to imply one of the following possibilities: first, that a regulation system other than angiogenesis was responsible for tumor growth, or, second, that because the dose of neutralizing anti-VEGF antibody was the same from day 7 to 27 after transplantation in our experimental protocol, it was insufficient against the grown cancer tissue from day 23 onward. Recently, antiangiogenic drugs have become expected to be a novel therapy for cancer. Some synthetic analogues of fumagillin inhibit angiogenesis and suppress the growth of many kinds of tumor in mouse models (Inger *et al.*, 1990). Some clinical trials of different angiogenesis inhibitors are already under way in the USA, UK and elsewhere in Europe, and extensive pre-clinical studies of angiogenesis inhibitors in animals have already been completed (Folkman, 1994). Quantitative methods developed to monitor the efficiency of antiangiogenic therapy are being tested in clinical trials. They include angiogenic peptide in serum, urine and cerebrospinal fluid, and quantitation of neovascularization in histological sections by microvessel count (Folkman, 1995). Depiction, quantitation and evaluation of angiogenic vessels in solid tumors are essential for evaluating the effects of these drugs. Microangiography has the advantage of allowing *in situ* analysis of angiogenic vessels and sequential changes in them. By contrast, conventional angiography cannot demonstrate these characteristic angiographic features well, and therefore does not allow evaluation of sequential changes in angiogenic vessels. Thus, our new synchrotron radiation microangiographic system allowed depiction and quantification of angiogenic vessels during the one to four weeks after transplantation in a mouse model. We were able to demonstrate the beneficial effects of antiangiogenic therapy with neutralizing antibody against vascular endothelial growth factor. Our synchrotron radiation microangiography system will be useful not only for basic research but also for clinical application.

5. Conclusions

Synchrotron microangiography was found to be useful for the depiction, quantification and evaluation of angiogenic vessels in cancer.

This work was supported by grants from the Japan Society for the Promotion of Science (JSPS-RFTF97I00201); New Energy and Industrial Technology Development Organization in Japan; Grants-in-aid for scientific research (07557060, 07807073, 09770961, 10470171) from the Ministry of Education, Science and Culture, Japan; Tokai University School of Medicine Research Aid; and 1998 Public Trust Fund for the Promotion of Surgery, Tokyo, Japan. This project was approved as a joint Research Program of the National Laboratory for High Energy Physics, Tsukuba, Japan (95G113, 95G287, 98G181, 98G194 and 98G195).

References

Ekelund, L. (1979). *Tumor Blood Circulation*, pp. 185–202. Florida: CRC Press.
Folkman, J. (1972). *Ann. Surg.* **175**, 409–416.
Folkman, J. (1990). *J. Natl Cancer Inst.* **82**, 4–6.
Folkman, J. (1994). *The Molecular Basis of Cancer.* Philadelphia: W. B. Saunders.
Folkman, J. (1995). *Nature Med.* **1**, 27–31.
Hermanek, P. & Sobin, L. H. (1987). *UICC TNM Classification of Malignant Tumors*, 4th ed., pp. 65–67. Berlin/Heidelberg/New York/London/Paris/Tokyo: Springer-Verlag.
Hyodo, K., Nishimura, K. & Ando, M. (1991). *Synchrotron Radiation Handbook*, pp. 55–94. Amsterdam: Elsevier Science.
Inger, D., Fujita, T., Kishimoto, S., Sudo, K., Kanamura, T., Brem, H. & Folkman, J. (1990). *Nature (London)*, **348**, 555–557.
Janet, E. W. H. & Julie, O. (1995). *Oxford Textbook of Oncology*, pp. 373–385. Oxford University Press.

Kim, K. J., Li, B., Winer, J., Armanini, M., Gillett, N., Phillips, H. S. & Ferrara, N. (1993). *Nature (London)*, **362**, 841–844.

Kubota, M., Kato, T., Suzuki, S., Maruyama, H. & Tanioka, K. (1996). *Soc. Photo-Opt. Instrum. Eng.* **2654**, 325–334.

Mori, H., Hyodo, K., Tanaka, E., Mohammed, M. U., Yamakawa, A., Shinozaki, Y., Nakazawa, H., Tanaka, Y., Sekka, T., Iwata, Y., Handa, S., Umetani, K., Ueki, H., Yokoyama, T., Tanioka, K., Kubota, M., Hosaka, H., Ishikawa, N. & Ando, M. (1996). *Radiology*, **201**, 173–177.

Mori, H., Hyodo, K., Tobita, K., Chujo, M., Shinozaki, Y., Sugishita, Y. & Ando, M. (1994). *Circulation*, **89**, 863–871.

Takeshita, S., Isshiki, T., Mori, H., Tanaka, E., Eto, K., Miyazaki, Y., Tanaka, A., Shinozaki, Y., Hyodo, K., Ando, M., Kubota, M., Tanioka, K., Umetani, K., Ochiai, M., Sato, T. & Miyashita, H. (1997). *Circulation*, **95**, 805–808.

Tanaka, A., Mori, H. & Tanaka, E. (1997). *Kokyu To Junkan*, **45**, 697–702. (In Japanese.)

Tanaka, A., Mori, H. & Tanaka, E. (1999). *Am. J. Physiol.* pp. H2263–H2268.

Tanioka, K., Yamazaki, J., Shidara, K. & Kawamura, T. (1988). *Advances in Electronics and Electron Physics*, pp. 379–387. New York: Academic Press.

Umetani, K., Ueki, H., Ueda, K., Hirai, T., Takeda, T., Doi, T., Wu, J., Itai, Y. & Akisada, M. (1996). *J. Synchrotron Rad.* **3**, 136–144.

Warren, B. A. (1979). *Tumor Blood Circulation*, pp. 1–47. Florida: CRC Press.